Check for updates

The FEBS Journal

FEBS PRESS science publishing by scientists

NOD1 cooperates with HAX-1 to promote cell migration in a RIPK2- and NF-κB-independent manner

Lucy Hezinger[1], Sarah Bauer[1], Kornelia Ellwanger[1], Alban Piotrowsky[2], Felix Biber[1], Sascha Venturelli[2,3] and Thomas A. Kufer[1]

1 Department of Immunology, Institute of Nutritional Medicine, University of Hohenheim, Stuttgart, Germany
2 Department of Biochemistry of Nutrition, University of Hohenheim, Stuttgart, Germany
3 Department of Vegetative and Clinical Physiology, Institute of Physiology, University Hospital Tuebingen, Germany

Keywords
cancer; chemotaxis; innate immunity; Nod-like receptors; RIPK2

Correspondence
T. A. Kufer, Department of Immunology, Institute of Nutritional Medicine, University of Hohenheim, Fruwirthstr.12, 70593 Stuttgart, Germany
Tel: +49 711 45-924850
E-mail: thomas.kufer@uni-hohenheim.de

(Received 9 February 2023, revised 13 June 2023, accepted 21 July 2023)

doi:10.1111/febs.16912

The human Nod-like receptor protein NOD1 is a well-described pattern-recognition receptor (PRR) with diverse functions. NOD1 associates with F-actin and its protein levels are upregulated in metastatic cancer cells. A hallmark of cancer cells is their ability to migrate, which involves actin remodelling. Using chemotaxis and wound healing assays, we show that *NOD1* expression correlated with the migration rate and chemotactic index in the cervical carcinoma cell line HeLa. The effect of NOD1 in cell migration was independent of the downstream kinase RIPK2 and NF-κB activity. Additionally, NOD1 negatively regulated the phosphorylation status of cofilin, which inhibits actin turnover. Co-immunoprecipitation assays identified HCLS1-associated protein X-1 (HAX-1) as a previously unknown interaction partner of NOD1. Silencing of *HAX-1* expression reduced the migration behaviour to similar levels as *NOD1* knockdown, and simultaneous knockdown of *NOD1* and *HAX-1* showed no additive effect, suggesting that both proteins act in the same pathway. In conclusion, our data revealed an important role of the PRR NOD1 in regulating cell migration as well as chemotaxis in human cervical cancer cells and identified HAX-1 as a protein that interacts with NOD1 and is involved in this signalling pathway.

Introduction

The innate immune system provides the first line of defence and reacts within minutes to hours to conserved structures of microorganisms, collectively called PAMPs (pathogen-associated molecular pattern), which are recognized by pattern-recognition receptors (PRRs) [1]. One important intracellular PRR is the nucleotide-binding and oligomerization domain (NOD)-like receptor (NLR) protein NOD1. NOD1 is activated by bacterial peptidoglycan fragments containing D-glutamyl-meso-diaminopimelic acid (IE-DAP) originating mainly from Gram-negative and certain Gram-positive bacteria [2,3]. Ligand binding induces homooligomerization of NOD1, which subsequently leads to the recruitment and activation of the receptor-interacting serine/threonine-protein kinase 2 (RIPK2) to induce nuclear factor κ-light-chain-enhancer of activated B cells

Abbreviations
AGC, automatic gain control; Arp, actin-related protein; Co-IP, co-immunoprecipitation; Dox, doxycycline; ECM, extracellular matrix; HAX-1, HCLS1-associated protein X-1; HPV, human papilloma viruses; IE-DAP, D-glutamyl-meso-diaminopimelic acid; MAPK, mitogen-activated protein kinase; MIT, maximum injection time; MS, mass spectrometry; NF-κB, nuclear factor κ-light-chain-enhancer of activated B cells; NLR, Nod-like receptor; NOD, nucleotide-binding and oligomerization domain; PAMP, pathogen-associated molecular pattern; PRR, pattern-recognition receptor; RIPK2, receptor-interacting serine/threonine-protein kinase 2; siNT, non-targeting siRNA; SSH1, slingshot homologue 1; TFA, trifluoroacetic acid; TNF, tumour necrosis factor; TriDAP, L-alanine-γ-D-glutamyl-meso-diaminopimelic acid; WT, wild-type.

This is an open access article under the terms of the Creative Commons Attribution-NonCommercial-NoDerivs License, which permits use and distribution in any medium, provided the original work is properly cited, the use is non-commercial and no modifications or adaptations are made.

(NF-κB) signalling [4] and activation of the mitogen-activated protein kinase (MAPK) pathway [5].

Besides its role as a PRR, NOD1 was reported to be associated with cancer progression. On the one hand, a protective role of NOD1 in cancer has been proposed as decreasing *NOD1* levels were correlated with tumour growth and progression of oestrogen sensitive breast cancer [6] and oral squamous cell carcinoma cells [7]. In *Nod1* knockout mice, inflammation-induced colon tumourigenesis was enhanced, the epithelial layer was more severely disrupted and more inflammatory cytokines were released compared to wild-type (WT) mice [8]. In cervical cancer, Liu *et al.* [9] hypothesized that the oncoproteins of human papilloma viruses (HPV) decrease NOD1 protein levels to inhibit NOD1-mediated apoptosis. On the contrary, more recent studies suggest a complex role of NOD1 in cancer progression. Zhang *et al.* reported that *NOD1* is highly expressed in HPV-induced malign cervix carcinoma, with *NOD1* expression correlating with reduced survival of the patients and increased proliferation, invasion and migration of the tumour cells. Additionally, basal IL-8 secretion was enhanced and the NF-κB and ERK signalling pathways were activated [10]. In ovarian cancer tissue, NOD1 and RIPK2 protein expression was shown to be upregulated, which was associated with a higher metastatic potential [11]. Mechanistically, *NOD1* expression increased the proliferation, invasion, NF-κB-mediated transcription and phosphorylation in a RIPK2-dependent manner [11]. Also, in colorectal cancer, NOD1 protein expression was reported to be highly elevated compared to control tissue [12], the protein level increased with cancer progression and was associated with shorter survival of the patients [13]. Additionally, NOD1 stimulation in colorectal cancer cells was shown to increase cell adhesion, migration and metastasis with involvement of the p38 MAPK pathway [13]. Interestingly, in myeloid cells, Maisonneuve *et al.* described a NOD1-induced immunosuppressive, tumour-tolerating micro-environment, thereby providing another mechanism for how NOD1 can promote tumour progression. In their study, systemic activation of NOD1 in mice resulted in reprogramming of macrophages towards an anti-inflammatory phenotype and expansion of myeloid-derived suppressor cells [14].

To conclude, several independent lines of evidence show that *NOD1* expression is associated with cancer progression and malignant transformation. The underlying mechanisms, however, are still poorly defined and might be cell type specific, thus explaining the partly contradictory findings.

HCLS1-associated protein X-1 (HAX-1) is a protein with multiple biological functions, including the stabilization of the mitochondrial membrane potential [15], the regulation of calcium storage in the sarcoplasmic reticulum [16], the stimulation of cell migration [17] and the inhibition of apoptosis [18]. Polymorphisms in *HAX-1* are associated with Kostmann's disease, a genetic form of agranulocytosis [19]. However, the exact biological function of HAX-1 in this disease remains still unknown. *HAX-1* is further overexpressed in several different cancer entities and its protein levels are positively associated with metastasis, cancer progression and cell growth and have a negative impact on survival of the patients. This was shown for colorectal cancer [20], oesophageal squamous cell carcinoma [21,22], lung cancer [23], melanoma [23], breast cancer [23], liver cancer [24,25] and ovarian cancer [26]. *HAX-1* knockdown reduced cell migration in hepatocellular [25], ovarian [26] and glioma [27] cancer cells. More specifically, in one study silencing of *HAX-1* did not attenuate single-cell migration, but collective cell migration, which was due to reduced cell–cell and cell–extracellular matrix (ECM) contacts [28]. All these studies support that the expression of *HAX-1* promotes cancer progression.

Cell migration is a highly regulated physiological process in multicellular organisms that is essential for embryonal development, vascularization and tissue repair. It is also used by malignant cancer cells for metastasis [29]. Cells can either migrate as individual cells (single-cell migration), which plays an important role in immune cell trafficking, or unidirectional as a group (collective cell migration), which takes place during wound healing. For collective cell migration, the connection of the cells through tight junctions is important [30,31]. Tumour cells use both single and collective cell migration for spreading and tissue invasion [30]. The speed of the migrating cell is mainly influenced by the turnover rate of F-actin polymerization and adhesion/deadhesion to the ECM [30]. Thereby F-actin polymerization and depolymerization are promoted by actin-related protein (Arp) 2/3 and cofilin respectively. The activity of cofilin is regulated by the protein phosphatase slingshot homologue 1 (SSH1) and LIM domain kinases 1 and 2 (LIMK1/2), whereas Arp2/3 requires cortactin, Rac family small GTPase 1 (Rac1) and Gα13 for its activity [17,32]. For NOD1 and HAX-1 diverse regulatory functions in the actin cytoskeleton remodelling have been described. NOD1 is known to enhance the activity of SSH1 [33] and interact with Rac1 [34], whereas HAX-1 was shown to complex with Rac1, cortactin and Gα13 [17,26] and to activate the Arp2/3 complex [35]. Besides, HAX-1 is required for junction complexes between the cells, which are important for collective

17424658, 2023, 22, Downloaded from https://febs.onlinelibrary.wiley.com/doi/10.1111/febs.16912 by Universität Hohenheim, Wiley Online Library on [09/09/2026]. See the Terms and Conditions (https://onlinelibrary.wiley.com/terms-and-conditions) on Wiley Online Library for rules of use; OA articles are governed by the applicable Creative Commons License

cell migration, and E-cadherin is delocalized in *HAX-1* deficient MCF7 cells. Additionally, HAX-1 is involved in the regulation of adhesion molecules to the ECM, which are enhanced upon *HAX-1* depletion [28]. Consequently, knockdown of *HAX-1* can impair the detachment and chemotactic migration of neutrophils [36]. Reduced cell-ECM adhesion was observed upon *NOD1* knockdown, while NOD1 stimulation induced ECM adhesion complexes, which directly influences cell migration in the colon cancer cell line HT29 [13].

Here, we provide evidence that expression of *NOD1* correlates with the migration rate and chemotaxis in HeLa cells. Co-immunoprecipitation (Co-IP) identified HAX-1 as a novel NOD1 interaction partner in HeLa cells and silencing of either *HAX-1* or *NOD1* reduced cell migration. The effect in cell migration was independent of NF-κB activation and RIPK2, the essential signalling partner for NOD1. The phosphorylation of cofilin, which inhibits actin turnover, was negatively regulated by NOD1. In conclusion, *NOD1* and *HAX-1* expression positively influenced cell migration and our data suggest that both might act in a common pathway.

Results

NOD1 expression enhances collective cell migration

NOD1 interacts with and activates SSH1, an enzyme promoting cell migration by enhancing the dephosphorylation of cofilin [33]. To investigate whether NOD1 influences cell migration, wound closure of cervical carcinoma HeLa cells was observed by microscopy in wound healing assays using automated gap recognition (Movie S1). HeLa cells with doxycycline (Dox)-inducible expression of *NOD1-eGFP* (NOD1-eGFP) showed an enhanced sheet migration behaviour compared to HeLa cells with inducible *eGFP* expression (Fig. 1A), whereas Dox treatment itself did not affect the migration behaviour of *eGFP* expressing HeLa cells (Fig. 1H). In order to corroborate the microscopy data, as a second readout we used the xCELLigence system that measures cell migration by assessing the impedance. Additional induction of *NOD1* expression by Dox slightly increased cell migration (Fig. 1B). Successful induction of *NOD1-eGFP* by Dox treatment in NOD1-eGFP cells was verified by immunoblot (Fig. 1C) and qPCR (Fig. 1D). Notably, a low leaky expression of *NOD1-eGFP* was detected also in untreated cells (Fig. 1C,D).

Next, we aimed to confirm the effect of NOD1 on cell migration by reducing *NOD1* expression. To this end, we transfected a NOD1-targeting siRNA in uninduced *NOD1-eGFP*-expressing HeLa cells. Silencing of the leaky *NOD1-eGFP* expression led to significantly reduced migration of NOD1-eGFP cells in the microscopy assay (Fig. 1E) and the xCELLigence system (Fig. 1F) as compared to a non-targeting siRNA control (siNT). Knockdown efficiency was confirmed by immunoblot (Fig. 1G). Importantly, targeting *eGFP* expression in Dox-induced or uninduced eGFP control cells did not change migration behaviour compared to siNT control (Fig. 1H), excluding an effect of *eGFP* expression on cell migration in our system. *eGFP* knockdown efficiency was verified by immunoblot (Fig. 1J). We also targeted *NOD1-eGFP* expression by the same eGFP-specific siRNA in NOD1-eGFP cells and measured migration by another well-established method (Tscratch). This showed that targeting *eGFP* reduced cell migration to similar extent as the *NOD1*-specific siRNA (Fig. 1I). Knockdown efficiency in this assay was verified by measuring eGFP fluorescence (Fig. 1K).

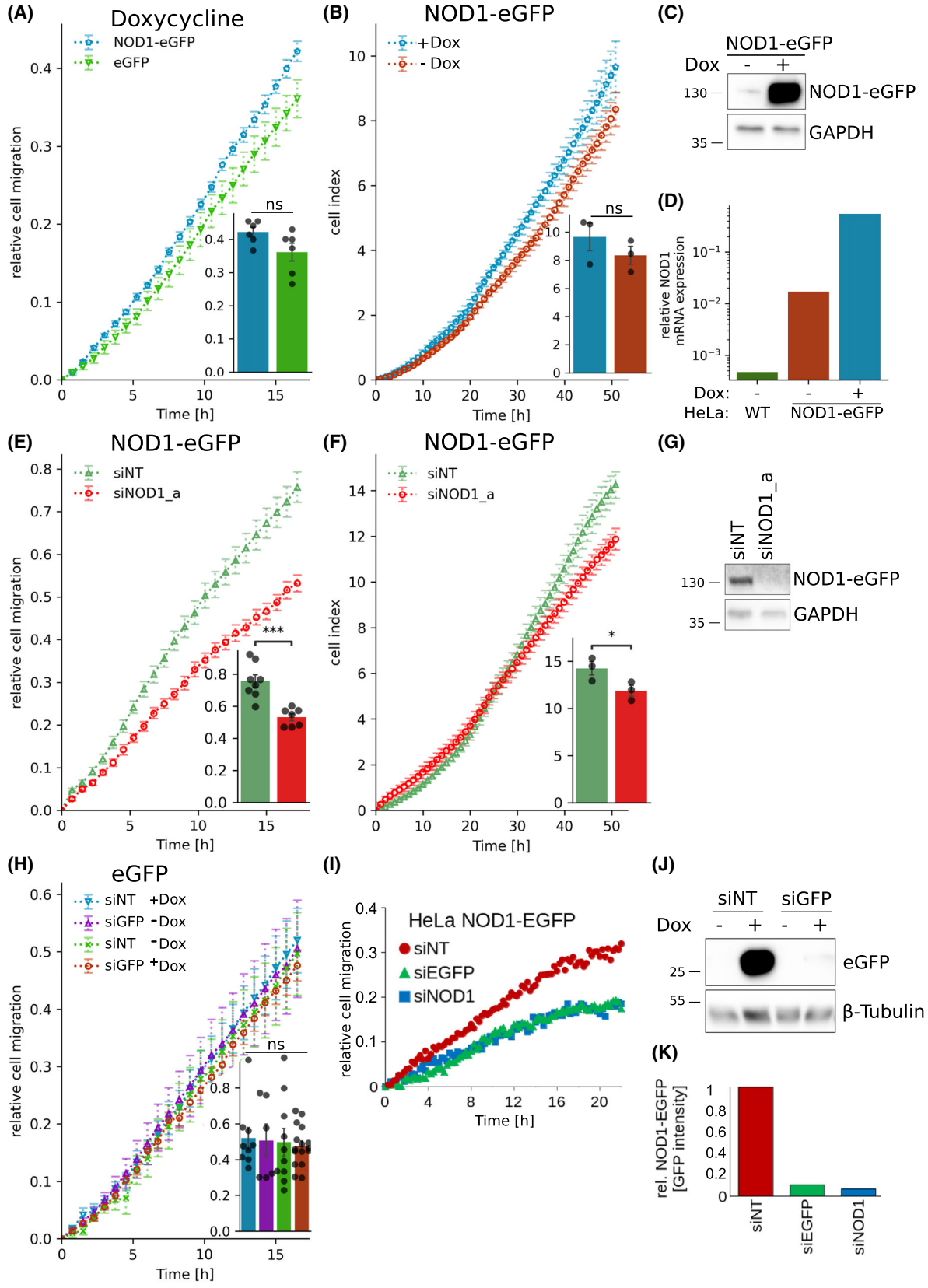
To further corroborate that the observed migration-enhancing effect was not an artefact of the stable HeLa Flp-In cell line used, the migration experiments were repeated using HeLa WT cells. *NOD1* knockdown significantly reduced the migration of HeLa cells in microscopy (Fig. 2A) and xCELLigence (Fig. 2B) assays. To exclude off-target effects of the siRNA, this effect was validated by another siRNA duplex targeting *NOD1* in the microscopy assay (Fig. 2A). Knockdown efficiency of both siRNAs was confirmed by qPCR (Fig. 2C).

In conclusion, our results provide significant evidence that *NOD1* expression enhances cell migration of HeLa cells.

NOD1 silencing impairs chemotaxis

To characterize the influence of NOD1 on single-cell migration, we assayed the effect of NOD1 on CXCL12 (C-X-C motif ligand)-mediated chemotaxis in HeLa cells [37–39]. To this end, a linear concentration gradient of the chemoattractant CXCL12 (aka SDF-1) was established across the cells using the μ-Slide chemotaxis chamber (Fig. 3A). The direction and speed of single cells were observed with live-cell imaging and compared between HeLa WT cells treated with NOD1-specific siRNA or siNT respectively. The relative path of 67 single *NOD1* silenced or control cells, which were observed for 24 h in the microscope, is presented in Fig. 3B. The total path length was comparable between control and *NOD1* knockdown cells [257 ± 13 μm versus 240 ± 14 μm (mean ± SEM)]

17424658, 2023, 22, Downloaded from https://febs.onlinelibrary.wiley.com/doi/10.1111/febs.16912 by Universität Hohenheim, Wiley Online Library on [09/09/2026]. See the Terms and Conditions (https://onlinelibrary.wiley.com/terms-and-conditions) on Wiley Online Library for rules of use; OA articles are governed by the applicable Creative Commons License



17424658, 2023, 22, Downloaded from https://febs.onlinelibrary.wiley.com/doi/10.1111/febs.16912 by Universität Hohenheim, Wiley Online Library on [09/09/2026]. See the Terms and Conditions (https://onlinelibrary.wiley.com/terms-and-conditions) on Wiley Online Library for rules of use; OA articles are governed by the applicable Creative Commons License

Fig. 1. Sheet migration is increased by *NOD1* expression. (A) Wound healing assay of Dox-induced HeLa NOD1-eGFP and eGFP cells. (B) Cell Index via impedance of Dox-induced HeLa NOD1-eGFP cells was measured. (C) Immunoblot of protein lysates from HeLa NOD1-eGFP cells induced with Dox, probed for eGFP and GAPDH. (D) *NOD1* mRNA expression of Dox-induced HeLa NOD1-eGFP and HeLa WT cells was analysed by qPCR and normalized to *GAPDH*. (E–G) siRNA-mediated silencing of *NOD1* expression in HeLa NOD1-eGFP cells. Knockdown with siNT was used as control. Cell migration was assessed by wound healing (E) or xCELLigence (F) assays. (G) Immunoblot of NOD1-eGFP cell protein lysates 96 h after transfection with siRNA, probed for GFP and GAPDH. (H) siRNA-mediated silencing of *eGFP* in Dox-induced HeLa eGFP cells. Cell migration was assessed by wound healing assays. (I) Wound healing assay of siNT, siNOD1_a and siGFP transfected HeLa NOD1-eGFP cells. Wound closure was analysed with Tscratch. (J) Immunoblot of protein lysates from (H), probed for GFP and β-tubulin. (K) Relative GFP intensity of HeLa NOD1-eGFP cells from (I). Differences between groups were assessed with Kruskal–Wallis test and if significant subsequently one-sided Mann–Whitney *U* test. ns, non-significant *P*-value > 0.05; $*P \leq 0.05$; $***P \leq 0.001$. Data are representative of two independent experiments. Data show mean ± SEM.

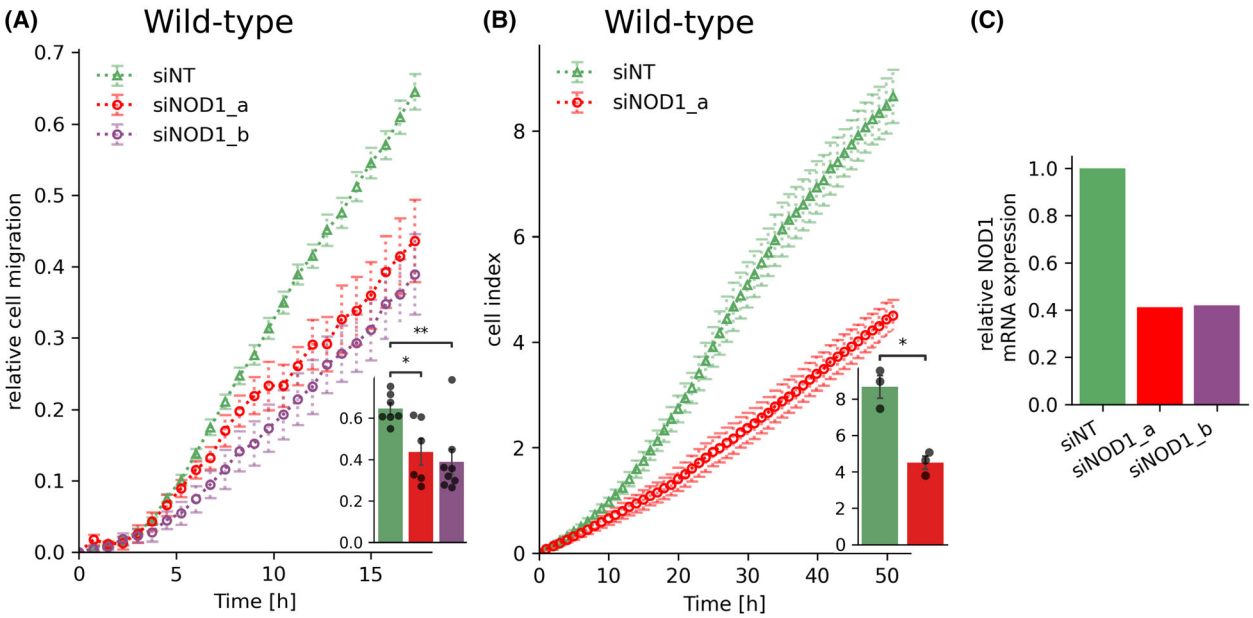


Fig. 2. Knockdown of *NOD1* reduces migration in HeLa WT cells. Cell migration of HeLa WT cells treated with *NOD1*-targeting or non-targeting (siNT) siRNAs was measured in wound healing (A) and xCELLigence assays (B). (C) *NOD1* mRNA expression of *NOD1* silenced HeLa WT cells was analysed by qPCR and normalized to *GAPDH*. Differences between groups were assessed with Kruskal–Wallis test and if significant subsequently one-sided Mann–Whitney *U* test. $*P \leq 0.05$; $**P \leq 0.01$. Data are representative of two independent experiments. Data show mean ± SEM.

(Fig. 3C), but the chemotactic index, which describes the path towards the chemoattractant in relation to the total migrated path, of the *NOD1* silenced cells was significantly lower compared to siNT-treated cells [0.132 ± 0.029 versus 0.342 ± 0.028 (mean ± SEM)] (Fig. 3D). On average, siNOD1_a treated cells migrated 38.6 ± 8.2 µm towards CXCL12 compared to 87.5 ± 9.3 µm (mean ± SEM) of cells treated with siNT (Fig. 3B).

These data show that *NOD1* knockdown not only reduced sheet but also chemotactic migration of HeLa cells.

HAX-1 interacts with NOD1

NOD1 was shown to interact with F-actin and to be recruited to the entry site of the bacterium *Shigella* at the plasma membrane in human cells [40]. Moreover, disturbances in actin dynamics and Rho GTPase activity result in NOD1-dependent NF-κB activation [33,34,40]. To find proteins that link NOD1 to actin and cell migration, we performed immunoprecipitation of NOD1 in HeLa NOD1-eGFP cells at steady-state condition and 0.5, 1 and 2 h postinfection with the Gram-negative bacterium *Shigella flexneri*, a well-

17424658, 2023, 22, Downloaded from https://febs.onlinelibrary.wiley.com/doi/10.1111/febs.16912 by Universität Hohenheim, Wiley Online Library on [09/09/2026]. See the Terms and Conditions (https://onlinelibrary.wiley.com/terms-and-conditions) on Wiley Online Library for rules of use; OA articles are governed by the applicable Creative Commons License

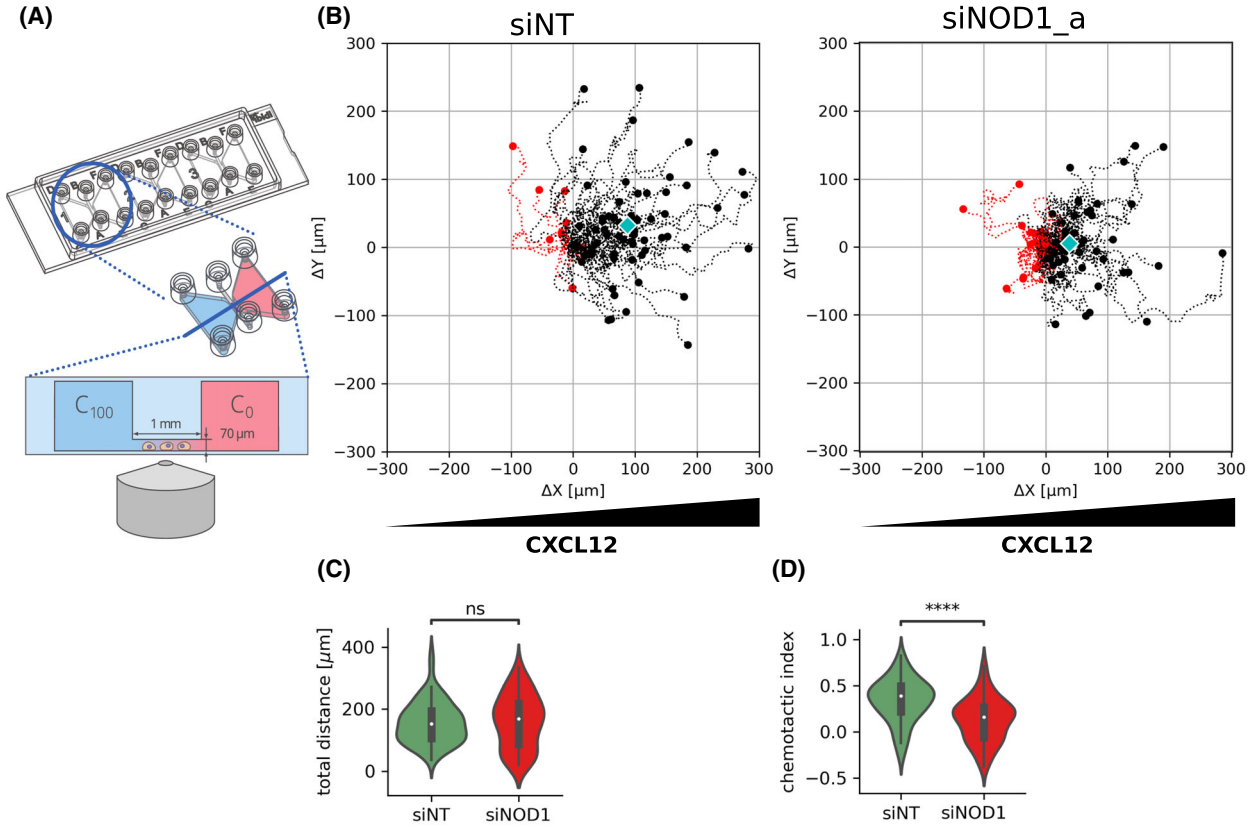


Fig. 3. Knockdown of *NOD1* negatively regulates chemotactic migration. (A) Schematic image of µ-Slide Chemotaxis (courtesy of ibidi GmbH). Cells were seeded in the growth area and one reservoir was filled with medium supplemented with chemoattractant or vehicle. (B) Relative migration plots of 67 HeLa WT cells 70 h after knockdown of *NOD1* or control knockdown with siNT. Concentration gradient of CXCL12 (50 nM) is indicated at the bottom of the graph. Cells were imaged every 30 min for 24 h and tracked manually. The mean of the endpoint of all tracked cells is represented by the blue diamond. Mean ± SEM. siNT: 87.5 ± 9.3 µm, siNOD1_a: 38.6 ± 8.2 µm. (C, D) Violin plot with mean of the cumulative distance (C) or chemotactic index (D) from single-tracked *NOD1* or control knockdown HeLa WT cell. One-sided *t*-test was applied, ****$P \leq 0.0001$; ns, non-significant $P > 0.05$. Data are representative of two independent experiments.

described NOD1 activator [41]. Proteins copurifying with NOD1-eGFP but not with eGFP used as a control were identified by mass spectrometry. Beside several heat-shock proteins, we identified HAX-1, an actin-associated protein, as one of the most abundant proteins to bind to NOD1. Interaction of HAX-1 and NOD1 was verified by immunoblot and was independent of *Shigella* infection (Fig. 4A). To map the domain of NOD1 responsible for the interaction, myc-HAX-1 was transiently overexpressed in HEK293T cells together with Flag-NOD1, Flag-NOD1ΔCARD or Flag-NOD1ΔLRR (Fig. 4B) respectively. Ectopically expressed myc-HAX-1 co-purified with all NOD1 constructs, but was not detected in the control condition lacking NOD1 expression (Fig. 4C). Interestingly, interaction of HAX-1 was increased upon deletion of the CARD and, even more pronounced, the LRR domain (Fig. 4C). For endogenous HAX-1, interaction with full-length NOD1 was very weak, however, as seen for the ectopically expressed myc-HAX-1 interaction was enhanced for Flag-NOD1ΔCARD and Flag-NOD1ΔLRR (Fig. 4D). These data show that the CARD and LRR domains in NOD1 are not necessary for the interaction but in fact might even hinder copurification of NOD1 and HAX-1.

Together this identifies HAX-1 as a novel interaction partner of NOD1.

HAX-1 knockdown decreases migration to the same extent as NOD1 knockdown

As HAX-1 was reported to play a role in cell migration [24] and is an interaction partner of NOD1, we next investigated the effect of HAX-1 on sheet migration. In wound healing assays with HeLa WT cells, knockdown of *HAX-1* by two different siRNAs

17424658, 2023, 22, Downloaded from https://febs.onlinelibrary.wiley.com/doi/10.1111/febs.16912 by Universität Hohenheim, Wiley Online Library on [09/09/2026]. See the Terms and Conditions (https://onlinelibrary.wiley.com/terms-and-conditions) on Wiley Online Library for rules of use; OA articles are governed by the applicable Creative Commons License

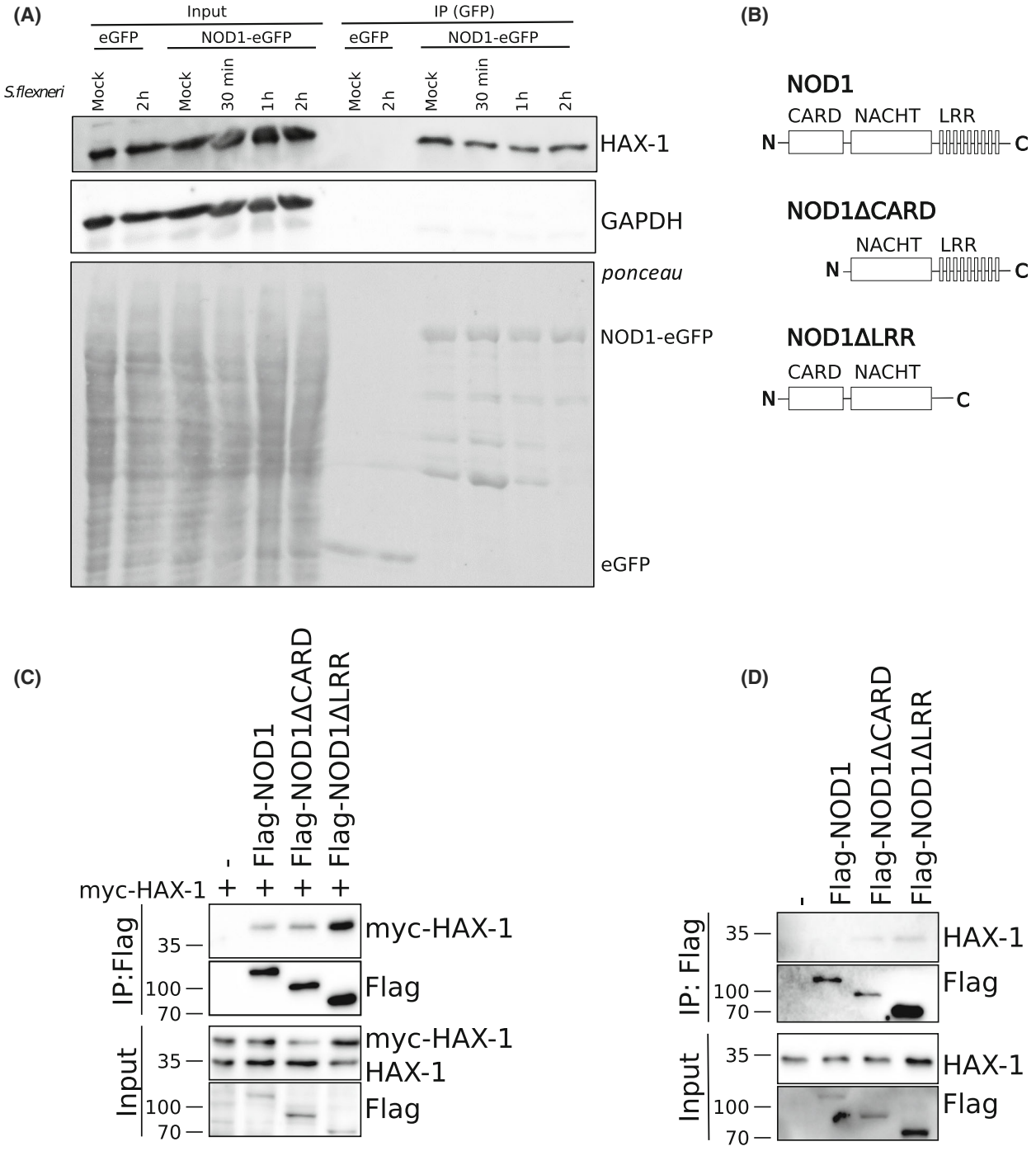


Fig. 4. HAX-1 is an interaction partner of NOD1. (A) Anti-GFP immunoprecipitation from *Shigella flexneri* infected HeLa NOD1-eGFP and eGFP cells. Immunoblot was probed for HAX-1 and GAPDH and ponceau staining is shown. (B) Schematic structure of NOD1 and NOD1 constructs used in (C, D). (C, D) HEK293T cells were transiently transfected with Flag-NOD1, Flag-NOD1ΔCARD or Flag-NOD1ΔLRR (C, D) and myc-HAX1 (C) and anti-Flag IP was performed. Immunoblots were probed for HAX-1 and Flag. Data are representative of two independent experiments.

confirmed a positive effect of HAX-1 on cell migration (Fig. 5A). Separate knockdown of *NOD1* and *HAX-1* thereby showed a comparable effect in the wound healing as well as in the xCELLigence assay (Fig. 5A, C) and double knockdown of both *NOD1* and *HAX-1* did not further decrease the migration rate in

17424658, 2023, 22, Downloaded from https://febs.onlinelibrary.wiley.com/doi/10.1111/febs.16912 by Universität Hohenheim, Wiley Online Library on [09/09/2026]. See the Terms and Conditions (https://onlinelibrary.wiley.com/terms-and-conditions) on Wiley Online Library for rules of use; OA articles are governed by the applicable Creative Commons License

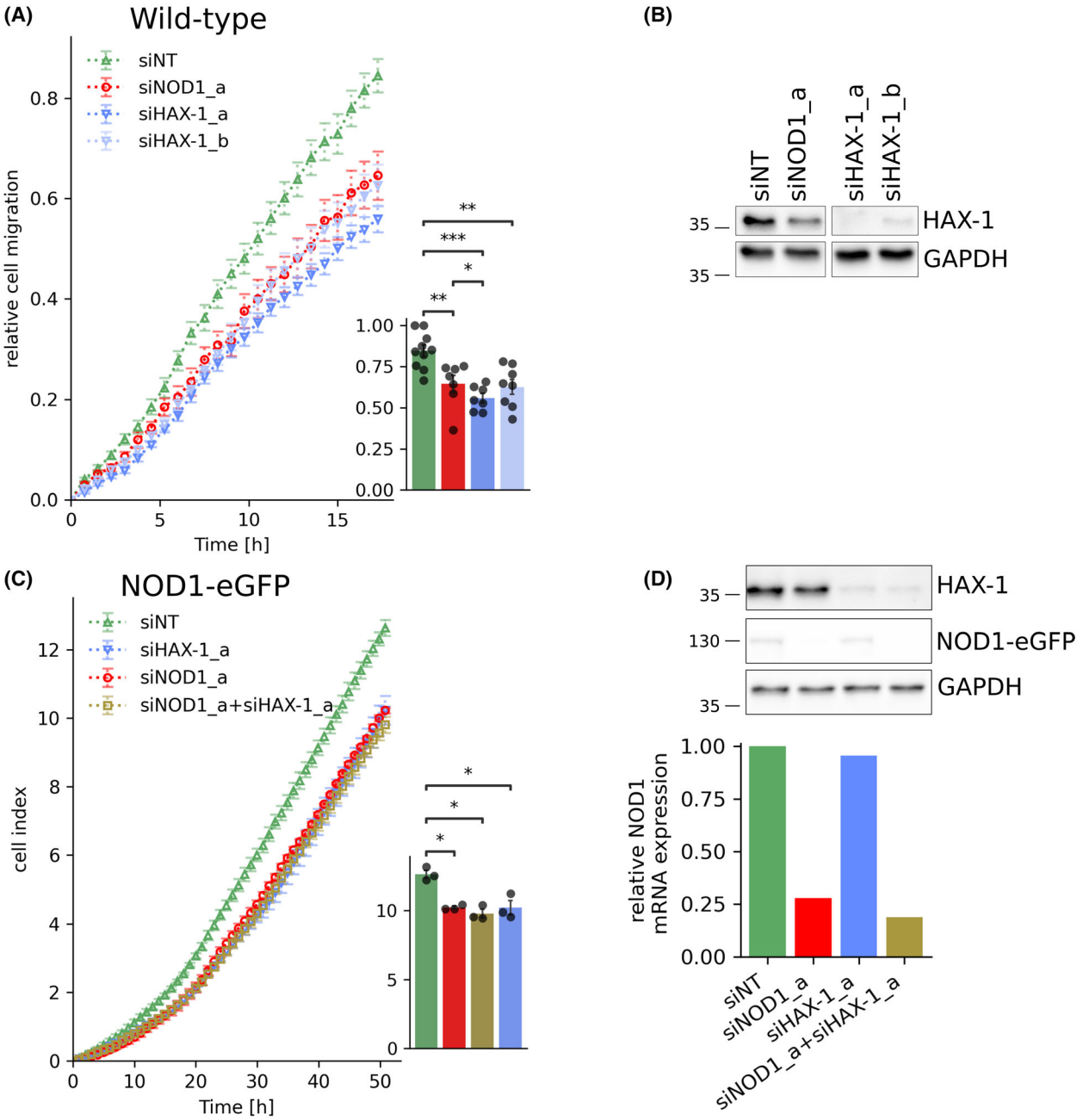


Fig. 5. Knockdown of *HAX-1* impairs migration, silencing of *NOD1* and *HAX-1* has no additive effect. (A) Wound healing assay of *NOD1* or *HAX-1* silenced HeLa WT cells. Knockdown with siNT was used as control. (B) Immunoblot analysis of cells from (A) 96 h after knockdown. Blot was probed for HAX-1 and GAPDH. (C) xCELLigence scratch assay of *HAX-1*, *NOD1* or *HAX-1* and *NOD1* silenced HeLa NOD1-eGFP cells. (D) Upper panel: Immunoblot of protein lysates of cells from (C) 68 h after siRNA transfection. Blot was probed for HAX-1, GFP and GAPDH. Lower panel: *NOD1* mRNA expression relative to *GAPDH* determined by qPCR 68 h after siRNA transfection. Differences between groups were assessed with Kruskal–Wallis test and if significant subsequently one-sided Mann–Whitney *U* test; $*P < 0.05$; $**P \leq 0.01$; $***P \leq 0.001$. Data are representative of two independent experiments. Data show mean ± SEM.

xCELLigence assays (Fig. 5C). Knockdown efficiency was validated by immunoblot analysis and qPCR (Fig. 5B,D).

Thus, our data strongly suggest *HAX-1* and *NOD1* expression to influence cell migration, however, not synergistically.

17424658, 2023, 22, Downloaded from https://febs.onlinelibrary.wiley.com/doi/10.1111/febs.16912 by Universität Hohenheim, Wiley Online Library on [09/09/2026]. See the Terms and Conditions (https://onlinelibrary.wiley.com/terms-and-conditions) on Wiley Online Library for rules of use; OA articles are governed by the applicable Creative Commons License

NOD1 and HAX-1 affect cell migration independently of RIPK2 and NF-κB activation

NOD1 overexpression in our HeLa NOD1-eGFP cells induces NF-κB activation [42] via RIPK2 and most NOD1-mediated effects require RIPK2 signalling [43]. However, also RIPK2 independent signalling of NOD1 has been described, such as for the induction of autophagy in some cells [44]. To test if NF-κB activation contributes to changes in cell migration in our model, HeLa eGFP cells were treated with increasing concentrations of tumour necrosis factor (TNF). No difference in cell migration was observed between the unstimulated and stimulated cells (Fig. 6A), besides TNF strongly induced IL-8 release indicative of NF-κB activation (Fig. 6B). Also, reduced migration was observed for *NOD1*-silenced HeLa WT cells, this was not affected by TNF treatment (Fig. 6C). *NOD1* knockdown was verified by qPCR (Fig. 6D) and by a reduction of IL-8 secretion after TNF stimulation (Fig. 6E). Thus, TNF stimulation does not affect the migration enhancing effect of NOD1 in HeLa cells, which strongly suggests this effect to be NF-κB independent.

As RIPK2 was reported to promote cell migration in vascular smooth muscle cells [45], we tested the influence of RIPK2 on cell migration. In HeLa WT cells, targeting *RIPK2* with two different siRNAs showed no effect on cell migration. In contrast, as shown above, siRNA-mediated knockdown of *NOD1* led to reduced cell migration (Fig. 6F). Both *RIPK2* siRNAs led to a significant reduction of RIPK2 protein levels as shown by immunoblot (Fig. 6G). To further exclude RIPK2 to play a role in NOD1-mediated cell migration, we additionally performed chemotaxis assays with *RIPK2* silenced HeLa WT and control cells and analysed the chemotactic migration towards the chemoattractant CXCL12 again using the μ-Slide chemotaxis chamber (Fig. 3A). The relative path of 50 single *RIPK2* silenced cells, which were observed for 24 h in the microscope, is presented in Fig. 6H. Successful chemotaxis was verified by Rayleigh test. No difference was observed in total path length [siNT: 117 ± 6 μm; siRIPK2: 116 ± 8 μm (mean ± SEM)] (Fig. 6I) or chemotactic index [siNT: 0.16 ± 0.05 μm; siRIPK2: 0.13 ± 0.05 μm (mean ± SEM)] (Fig. 6J) between *RIPK2* silenced and siNT control cells. Successful *RIPK2* knockdown was verified by immunoblot (Fig. 6K). Thus, the effect of NOD1 on migration is independent of RIPK2-mediated signalling.

Taken together, these experiments indicate that the observed migration enhancing effect in HeLa cells is independent of RIPK2 signalling and NF-κB activation.

NOD2 is a protein highly related to NOD1 both in structure and function and also signals by the activation of RIPK2 and NF-κB signalling [46,47]. *NOD2-eGFP* expressing HeLa cells, however, did not increase sheet migration compared to the HeLa eGFP cell line, even after induction of *NOD2-eGFP* expression by Dox (Fig. 7A). Successful induction of NOD2-eGFP was verified by immunoblot (Fig. 7B).

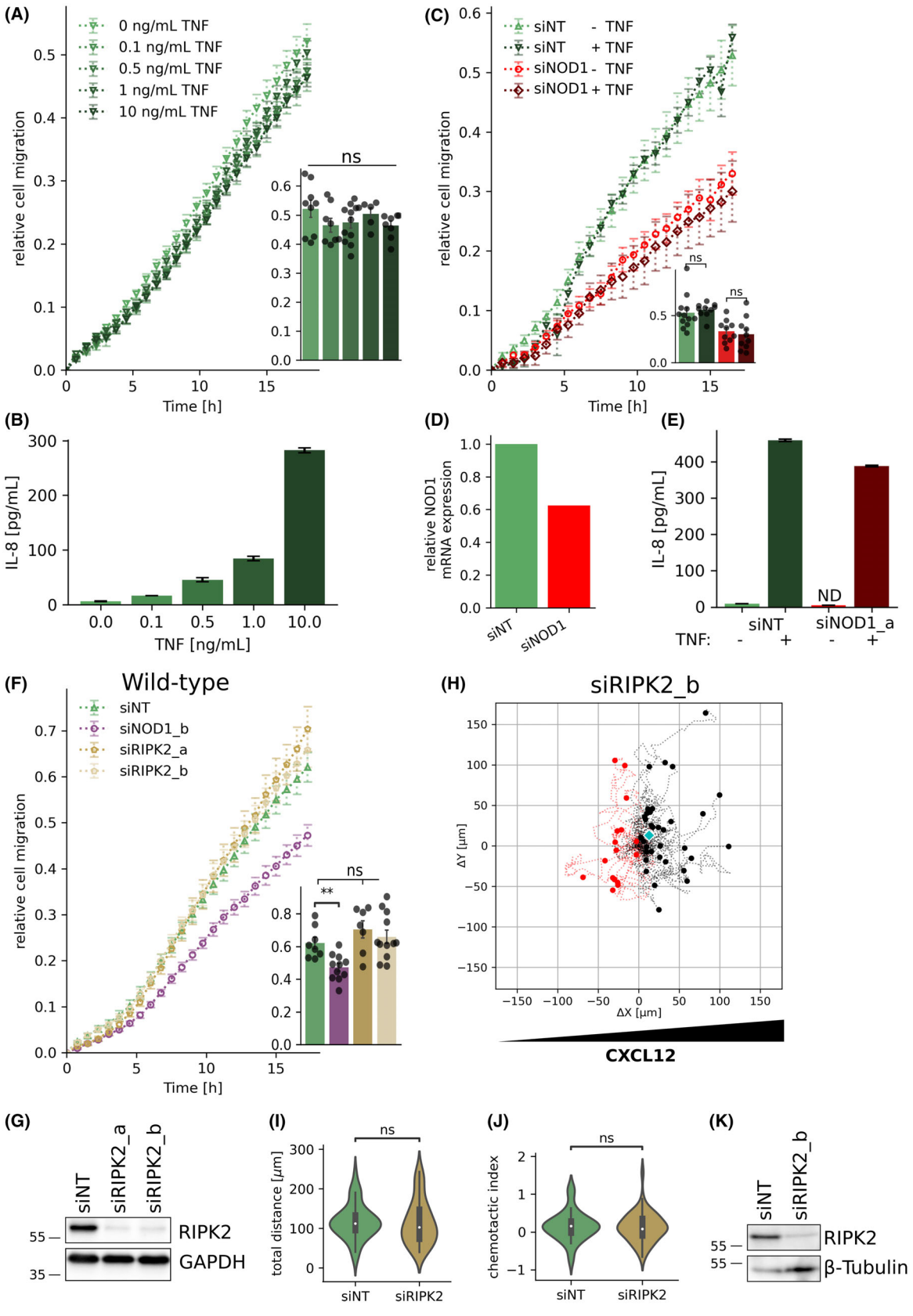
As neither NF-κB activation nor RIPK2-mediated signalling was involved in the NOD1-mediated migration enhancing effect, we ultimately assessed the effect of direct NOD1 stimulation on migration by wound healing assays. To this end, we stimulated HeLa WT cells with TriDAP (L-Ala-γ-D-Glu-mDAP), the specific agonist for NOD1, after scratching. NOD1 stimulation did not significantly alter cell migration compared to unstimulated cells (Fig. 7C). However, a small tendency towards enhanced cell migration was observed. Successful NOD1 activation by TriDAP stimulation was assessed by IL-8 release (Fig. 7D). These data suggest that the effect of NOD1 on cell migration is intrinsic rather than signalling mediated.

Phospho-cofilin (p-cofilin) promotes actin turnover by depolymerizing F-actin [32] and we showed earlier that NOD1 stimulation decreases p-cofilin levels [33]. In line with these findings, we observed that *NOD1* knockdown increased phosphorylation of cofilin at serine 3 in HeLa cells, whereas *HAX-1* knockdown had no measurable influence on the p-cofilin signal and *RIPK2* only slightly affected cofilin phosphorylation (Fig. 7E). These data might point towards an involvement of cofilin in the NOD1-, but not the HAX-1-mediated enhanced migration of HeLa cells, which in turn would indicate NOD1 and HAX-1 to be implicated in different branches of the same signalling pathway.

Discussion

Here, we show that *NOD1* expression correlates with cell migration in human cervical carcinoma cells. Using HeLa cells with inducible expression of *NOD1-eGFP*, we found that a very low (leaky) *NOD1-eGFP* expression already was sufficient to augment migration, whereas strong expression of *NOD1* had only a slight additional effect. The basal *NOD1* mRNA expression in HeLa WT cells is about 3% of the leaky expression of *NOD1* in HeLa NOD1-eGFP cells, whereas Dox treatment upregulated *NOD1* mRNA about 32-fold. This suggests that mild upregulation of *NOD1* is sufficient to reach saturation for the effect on cell migration, which is in line with the overall low

17424658, 2023, 22, Downloaded from https://febs.onlinelibrary.wiley.com/doi/10.1111/febs.16912 by Universität Hohenheim, Wiley Online Library on [09/09/2026]. See the Terms and Conditions (https://onlinelibrary.wiley.com/terms-and-conditions) on Wiley Online Library for rules of use; OA articles are governed by the applicable Creative Commons License



17424658, 2023, 22, Downloaded from https://febs.onlinelibrary.wiley.com/doi/10.1111/febs.16912 by Universität Hohenheim, Wiley Online Library on [09/09/2026]. See the Terms and Conditions (https://onlinelibrary.wiley.com/terms-and-conditions) on Wiley Online Library for rules of use; OA articles are governed by the applicable Creative Commons License

Fig. 6. NOD1 and HAX-1 influence on cell migration is independent of NF-κB and RIPK2. (A) Wound healing assay of HeLa eGFP cells stimulated with indicated concentrations of TNF after scratching. (B) IL-8 ELISA with supernatant of cells from (A) 24 h after stimulation. (C) Wound healing assay of HeLa WT cells after siRNA-mediated silencing of *NOD1* or control knockdown with siNT and treatment with the indicated concentrations of TNF after scratching. (D) *NOD1* mRNA expression relative to *GAPDH* of cells from (C) determined by qPCR 68 h after siRNA transfection. (E) IL-8 ELISA of supernatants from cells from (C) 24 h after stimulation. (F) Wound healing assay of *NOD1* or *RIPK2* silenced HeLa WT cells. (G) Immunoblot of protein lysates of cells from (F) 96 h after siRNA transfection. Blot was probed for RIPK2 and GAPDH. (H) Relative migration plots of 50 HeLa WT cells 70 h after knockdown of *RIPK2*. Concentration gradient of CXCL12 (50 nM) is indicated at the bottom of the graph. Cells were imaged every 30 min for 24 h and tracked manually. The mean of the endpoint of all tracked cells is represented by the blue diamond. Mean ± SEM 13 ± 5.2 μm. (I, J) Violin plot with mean of the cumulative distance (I) or chemotactic index (J) from single-tracked *RIPK2* or control knockdown HeLa WT cells. (K) Immunoblot of protein lysates of cells from (H). Blot was probed for RIPK2 and β-tubulin. Differences between groups were assessed with Kruskal–Wallis test and if significant subsequently one-sided Mann–Whitney *U* test. ns, non-significant *P*-value > 0.05; $^{**}P \leq 0.01$. Data are representative of 3 (C–E), 2 (A, B, F, G) or 1 (H–K) experiments. Data show mean ± SEM (A, C, F) or mean ± SD (B, E).

endogenous expression levels of *NOD1* and our observations on the effect of NOD1 in innate immunity where also low levels are sufficient to induce a robust immune response [40,42]. A role for NOD1 in cell migration has been reported also for cervical squamous cell carcinoma cells [10] and ovarian cancer cell lines [11] supporting our finding in the cervical carcinoma cell line HeLa. Controversial roles for NOD2 have been reported in cancer progression [12,48] and cell migration [10,49], whereas we could not confirm a robust effect of *NOD2* overexpression on cell migration in HeLa cells. These discrepancies might depend on differences in expression level and the cellular systems used.

Upon analysis of CXCL12 chemotaxis of HeLa cells, we found that the directed migration towards CXCL12 was impaired in *NOD1*-depleted cells. Interestingly, only the chemotactic index was decreased in *NOD1* silenced HeLa cells, but the total distance did not differ significantly between control and *NOD1* knockdown cells (Fig. 3). Fernández-García *et al.* and Kasimetty *et al.* reported diminished chemotaxis of neutrophils into the spleen of *Nod1* knockout mice in high-fat diet-induced atherosclerosis, and into the kidneys in ischemic kidney disease respectively [50,51]. This effect of NOD1 on chemotaxis was cell type specific, as monocyte/macrophage recruitment to the spleen was not affected [50]. Chan *et al.*, however, showed that the reason for reduced high-fat diet-induced neutrophil infiltration in adipose tissue in *Nod1* knockout mice likely is a diminished Cxcl1 production, as they did not observe changes in neutrophil chemotaxis towards Cxcl1 in *Nod1*-depleted neutrophils [52].

Our data support the conclusion that the effect of NOD1 on cell migration was independent of *RIPK2* expression which is in contrast to the results from Zhang *et al.* [45]. Possible explanations for this discrepancy might be the use of different cell lines or assays used to determine migration. Zhang *et al.* [45] utilized a Boyden chamber, which does not analyse collective sheet migration, but cell motility and invasion, whereas for this work, wound healing assays were used. NOD1 stimulates NF-κB activation through RIPK2 and the migration-enhancing effect of NOD1 was suggested to be mediated partly by p65 phosphorylation and MAPK activation [10]. However, TNF which activates both pathways did not influence the migration rate of HeLa cells in our study. The connection between NOD1-mediated activation of NF-κB and MAPK and cell migration thus likely is not causal. As also direct stimulation of NOD1 by its specific agonist did not significantly affect migration of HeLa cells, an intrinsic rather than a signalling-dependent role of NOD1 in the migration of epithelial carcinoma cells seems likely.

In this work, we identified HAX-1 as a novel interaction partner of NOD1. The interaction between NOD1 and HAX-1 was independent of *Shigella* infection and did not depend on the LRR or CARD domain of NOD1, suggesting an interaction of HAX-1 with the NACHT domain of NOD1. Interestingly, the interaction with HAX-1 seems to be stronger for NOD1 mutants lacking these domains (Fig. 4), suggesting a different conformation with better accessibility of HAX-1 binding sites for the CARD- and LRR-deficient constructs.

In line with the literature, silencing of *HAX-1* attenuated cell migration in our HeLa cell model [25–28]. Additional knockdown of *NOD1* did not further decrease cell migration. This provides first indirect evidence that NOD1 and HAX-1 might act in the same pathway, albeit further work is needed to prove this formally.

NOD1 knockdown increased p-cofilin levels in HeLa cells and simultaneously led to a reduction of total cofilin. This result is in line with the p-cofilin-reducing effect of NOD1 stimulation, which was reported by us

17424658, 2023, 22, Downloaded from https://febs.onlinelibrary.wiley.com/doi/10.1111/febs.16912 by Universität Hohenheim, Wiley Online Library on [09/09/2026]. See the Terms and Conditions (https://onlinelibrary.wiley.com/terms-and-conditions) on Wiley Online Library for rules of use; OA articles are governed by the applicable Creative Commons License

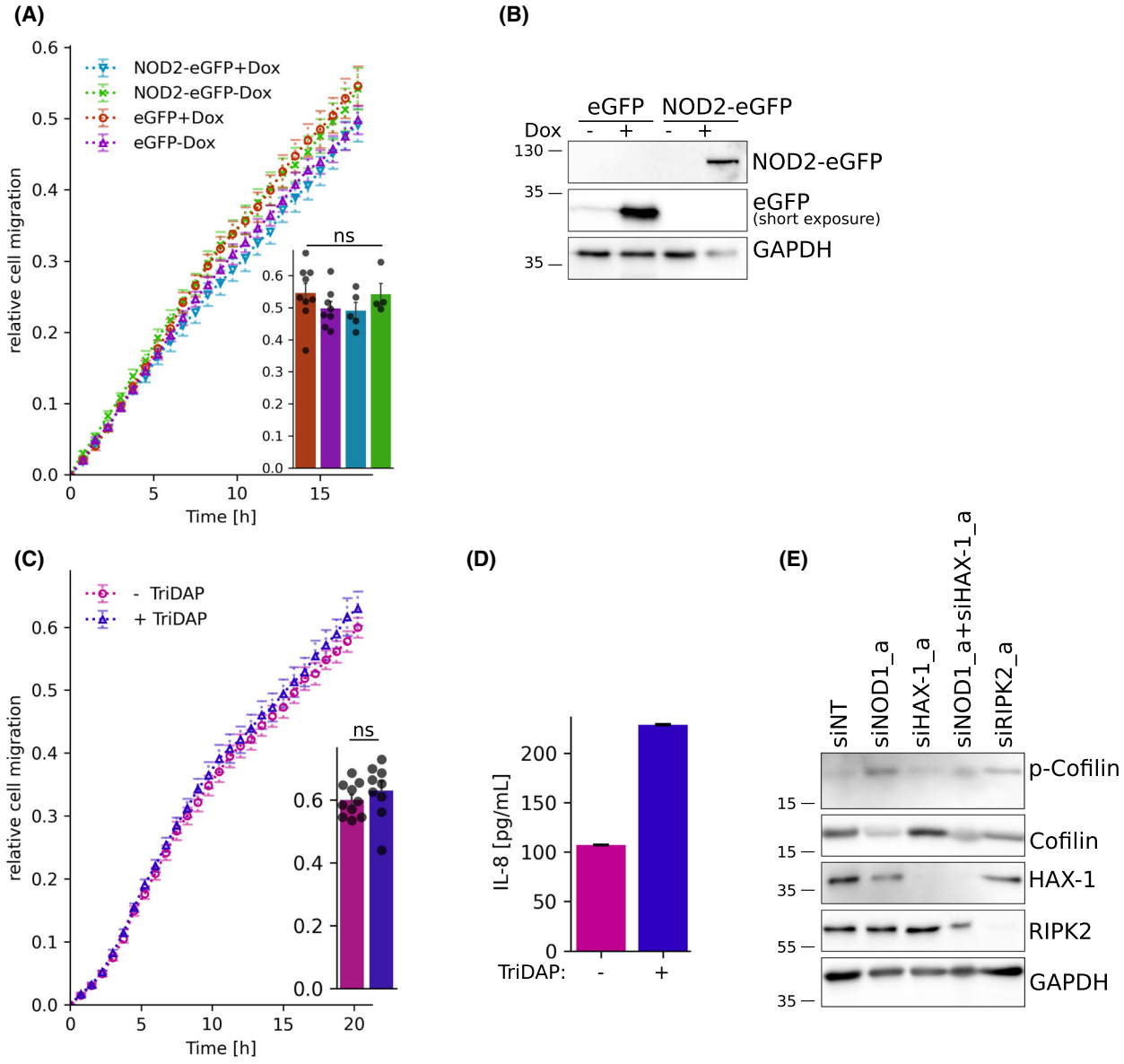


Fig. 7. Direct NOD1 stimulation does not affect cell migration. (A) Wound healing assay of Dox treated HeLa NOD2-eGFP and eGFP cells. (B) Immunoblot of protein lysates of cells from (A) 24 h after scratching. Blot was probed for eGFP and GAPDH. (C) Wound healing assay of HeLa WT cells stimulated with 20 μM L-Ala-γ-D-Glu-mDAP (TriDAP) after scratching. (D) IL-8 ELISA with supernatants of cells from (C) 24 h after stimulation. (E) Immunoblot of protein lysates of HeLa WT cells after 96 h knockdown of the indicated target or control knockdown with siNT. Blot was probed for p-cofilin, cofilin, HAX-1, RIPK2 and GAPDH. Differences between groups were assessed with Kruskal–Wallis test. ns, non-significant *P*-value > 0.05. Data are representative of at least two independent experiments. Data show mean ± SEM (A, C) or mean ± SD (D).

recently [33]. *HAX-1* knockdown did not affect p-cofilin and knockdown of *RIPK2* resulted only in a slight increase of p-cofilin, at best (Fig. 7E). As *RIPK2* silenced cells presented with increased p-cofilin levels but sheet and chemotactic migration was not impaired, it seems possible that NOD1 influences another, RIPK2-independent pathway to promote cell migration.

In the wound healing assays, the migration rate of cells with silenced *NOD1* expression was significantly reduced, but the total path of single-cell migration in chemotactic assay was only slightly diminished in *NOD1* knockdown cells. One possibility explaining the difference in the NOD1 dependency of migration might be that NOD1 regulates the junction proteins between cells like E-cadherin. The chemotaxis assay

17424658, 2023, 22, Downloaded from https://febs.onlinelibrary.wiley.com/doi/10.1111/febs.16912 by Universität Hohenheim, Wiley Online Library on [09/09/2026]. See the Terms and Conditions (https://onlinelibrary.wiley.com/terms-and-conditions) on Wiley Online Library for rules of use; OA articles are governed by the applicable Creative Commons License

analyses junction protein independent single-cell migration, whereas during the wound healing experiments, the cells are connected to the neighbour cells and migrate as one sheet. Disturbances in the localization of the junction proteins have been shown to slow down sheet migration [30]. For HAX-1, a similar phenomenon was reported. Balcerak *et al.* could show that *HAX-1* expression increased the junction proteins between the cells and simultaneously decreased the adhesion to the ECM. Therefore, *HAX-1* knockdown reduced collective but not single-cell migration [28]. NOD1 might regulate cell junction proteins important for cell migration. This would explain, why we did not see an effect of classical pro-inflammatory, RIPK2 and NF-κB-mediated NOD1 signalling on cell migration. Absence of NOD1 might lead to dysregulated cell junction protein expression and cytoskeletal dynamics, thus hampering coordinated cell–cell detachment and reattachment needed for efficient sheet migration. As overexpression and direct stimulation of NOD1 slightly, but not significantly enhanced cell migration, very small amounts of NOD1 might be sufficient to influence cell–cell adhesion molecules. Supporting this idea, we found *NOD1* silenced HeLa cells to adhere much stronger to the surface of cell culture vessels and to present with altered morphology compared to siNT control cells. In contrast, no altered detachment behaviour for the stable NOD1-eGFP cell line was observed (data not shown). Further speaking for NOD1 regulating cell junction proteins is our observation of increased phosphorylation of cofilin (Fig. 7E) and paxillin (data not shown), proteins involved in actin cytoskeletal remodelling and focal adhesion, respectively, in *NOD1* silenced HeLa cells. To clarify a potential role of NOD1 in regulating cell adhesion molecules should be subject to future studies.

Taken together, we show that NOD1 promotes cell migration in human cervical cancer cells. Thus, targeting NOD1 in epithelial cancer might be promising to reduce migration and cancer metastasis formation.

Materials and methods

Cells and cell culture

HEK293T (RRID:CVCL_0063) and HeLa cells (RRID: CVCL_0030) were obtained from ATCC and validated by multiplex human cell authentication test (Multiplexion, Friedrichshafen, Germany). Stable Dox-inducible HeLa cells expressing eGFP, NOD1-eGFP and NOD2-eGFP were described earlier [42,53]. All cell lines were cultivated in DMEM (Gibco, Life Technologies GmbH, Darmstadt, Germany) with 10% FBS (Biochrom AG, Berlin, Germany) and 1% Penicillin–Streptomycin (Gibco) at 37 °C and 5% CO_2 in a humid environment. 1 $\mu g \cdot mL^{-1}$ Dox was used to induce the overexpression of eGFP and eGFP fusion proteins for 20–24 h before the experiment. Cells were routinely checked for absence of mycoplasma contamination by PCR.

siRNA-mediated gene silencing

For gene silencing, 20 nM siRNA was transfected in HeLa cells using HiPerFect transfection reagent (Qiagen, Hilden, Germany) according to the manufacturer's instructions for 48 h before cells were seeded for further experiments. All siRNAs were purchased from Qiagen: siNOD1_a (Hs_CARD4_4), siNOD1_b (Hs_CARD4_5), siHAX-1_a (Hs_HAX1_6), siHAX-1_b (Hs_HAX1_6), siRIPK2_a (Hs_RIPK2_6), siRIPK2_b (Hs_RIPK2_8), siGFP (#1022064; Qiagen) and siNT (AllStars Negative Control).

Plasmid transfection

Transient overexpression of myc-HAX-1 [54], Flag-NOD1, Flag-NOD1ΔCARD, Flag-NOD1ΔLRR [40] or pcDNA (Invitrogen, Thermo Fisher Scientific, Darmstadt, Germany) as control was achieved by lipofection using Lipofectamine 2000 (Thermo Fisher Scientific) according to manufacturer's protocol. For this aim, cells were seeded in 24-well plates or 6-cm dishes and transfected with 250 or 500 ng plasmid, respectively, and used 20–24 h posttransfection.

PAMP and cytokine treatment

To induce NF-κB or NOD1 activation, medium supplemented with indicated concentration of TNF (Invivogen) or 20 μM TriDAP (Invivogen) was added to the cells directly after the scratch and before microscopy. To control for activation, supernatant of unscratched cells was taken 24 h after stimulation.

Immunoblotting

Cells were lysed in Laemmli SDS buffer followed by denaturation of the proteins for 5 min at 95 °C. Proteins were separated by Tris-Glycine SDS/PAGE and then transferred onto a 0.2-μm nitrocellulose membrane. Blocking was performed with 0.5% Roche Blocking reagent in PBS, followed by incubation with the appropriate primary antibody: anti-cofilin (5175P; Cell Signaling Technology, Leiden, The Netherlands; 1 : 1000), anti-Flag (F7425; Sigma-Aldrich, Merck, Darmstadt, Germany; 1 : 2000), anti-GFP (11814460001; Sigma-Aldrich; 1 : 2000), anti-HAX-1 (PA5-27592; Thermo Fisher, Darmstadt, Germany; 1 : 1000), anti-myc (M4439-100UL; Sigma-Aldrich; 1 : 400), anti-RIPK2 (75257; Abcam, Cambridge, UK; 1 : 1000), anti-p-Cofilin (3313S; Cell Signalling, Leiden, The Netherlands; 1 : 1000) and anti-GAPDH

17424658, 2023, 22, Downloaded from https://febs.onlinelibrary.wiley.com/doi/10.1111/febs.16912 by Universität Hohenheim, Wiley Online Library on [09/09/2026]. See the Terms and Conditions (https://onlinelibrary.wiley.com/terms-and-conditions) on Wiley Online Library for rules of use; OA articles are governed by the applicable Creative Commons License

(sc-25778; Santa Cruz, Heidelberg, Germany; 1 : 1000) or anti-beta-tubulin (ab15568; Abcam, Cambridge, UK; 1 : 1000) as loading control. For detection of primary antibodies, HRP-conjugated anti-rabbit IgG (170-6515; Bio-Rad, Feldkirchen, Germany), light-chain specific HRP-conjugated anti-mouse IgG (115-035-174; Jackson Immuno Research, Cambridgeshire, UK) and HRP-conjugated anti-mouse IgG (170-6516; Bio-Rad) were used. For signal detection, home-made ECL, Clarity Western ECL Substrate (Bio-Rad) or SuperSignal West Femto maximum sensitivity substrate (Thermo Fisher Scientific) were used and signals were recorded on an automated high-sensitivity CCD camera system (Fusion FX; Vilber Lourmat, Marne-La-Valée, France). Protein size was determined by running a standard indicating size in kDa.

Determination of fluorescence intensity

Knockdown efficiency of eGFP was partly determined by the measurement of the GFP fluorescence intensity at wavelength 488 nm using a multiplate reader (Envision, Perkin Elmer, Rodgau-Jügesheim, Germany).

Quantitative RT-PCR

For qPCR, cells were lysed 72 h after knockdown and the RNA was isolated using the RNeasy Plus Mini Kit (Qiagen) according to the manufacturer's instructions. The RNA was transcribed to cDNA with the iScript cDNA synthesis kit (Bio-Rad). qPCR was conducted using the GreenMasterMix kit (Genaxxon Bioscience, Ulm, Germany). The following primers were used: GAPDH (GGTATCGTGGAAGGACTCATGAC, ATGCCAGTGAGCTTCCCGTTCAG), NOD1 (TCCAAAGCCAAACAGAAACTC, CAGCATCCAGATGAACGTG). Relative expression to GAPDH was calculated using the Δcq method and for the knockdown experiments, relative expression was normalized to the siNT control.

Wound healing assay

To measure the migration behaviour, 7.5×10^4 Hela cells per well were seeded in a 48-well plate. For knockdown experiments, cells were harvested after 48 h. When indicated, 1 $\mu g \cdot mL^{-1}$ Dox was added to the medium. After the adhesion time of 24 h when the cell layer reached a confluency of 90%, the cell layer was scratched with a 10-μL pipette tip. Then, the cells were washed twice with sterile PBS, before 500 μL of culture medium was added for microscopy. The gap in the cell layer was monitored using live-cell imaging with a DMi8 inverted microscope (Leica, Wetzlar, Germany), equipped with an automated stage and an incubation system set to 37 °C and 5% CO_2. Using a 20× objective (HC Fluotar L 20×/0.40 DRY, Leica), 2–12 positions along the gap were defined for each condition, from which every 15 min for 18 h phase-contrast images were taken. After microscopy, cells were lysed for immunoblot analysis. The exported time series were analysed in IMAGEJ using the macro MRI_WHT_KuferLabHohenheim (https://github.com/KuferLabHohenheim/Woundhealing-Tool.git) which is a usability improved version from MRI Wound healing tool [55] (Settings: method: variance; variance filter radius: 10; radius open: 10; minimum size: 10 000). The observed open area at each time point was normalized to the initial open area and subtracted from one to display the relative migration. Alternatively, images were analysed using Tscratch (CSE-lab) [56].

xCELLigence measurement

After 48 h of knockdown, 1.5×10^4 or 2×10^4 Hela WT or HeLa NOD1-eGFP cells were seeded into each well of an E-Plate WOUND 96 (Agilent Technologies, Inc., Waldbronn, Germany) and treated with 1 $\mu g \cdot mL^{-1}$ Dox when indicated. After an adhesion time of 19 h, the cell layer was scratched with the AccuWound 96 Scratch Tool (Agilent Technologies, Inc.). Before the E-Plate was placed in the xCELLigence RTCA device (Agilent Technologies, Inc.), the cells were washed once with PBS and 200-μL culture medium was added. The impedance depicted as unitless Cell Index in the scratch area was then measured every 15 min for 53 h in three wells per condition. Every fourth data point was then plotted. Mean and SEM of technical triplicates are shown in the figures.

Chemotaxis assay

Forty-eight hours after siRNA treatment, 6 μL of a 2×10^6 per mL HeLa cell suspension in DMEM with 10% FBS and 20 mM HEPES was transferred into the middle chamber of a μ-Slide Chemotaxis (Ibidi, Gräfelfing, Germany) according to manufacturer's instructions. For cell attachment, the slide was placed in a humidity chamber for 16 h at 37 °C, 5% CO_2, before the medium in the slide was changed to chemotaxis medium (DMEM with 1% FBS and 20 mM HEPES). After 6 h, the reservoirs were filled with chemotaxis medium and two times 16.25 μL of 100 nM CXCL12 (PeproTech, Thermo Fisher Scientific, Hamburg, Germany) was applied to the right side to reach a final concentration of 50 nM CXCL12 in the slide. Movement of the cells was recorded at 37 °C and 5% CO_2 by phase-contrast imaging. Eight overlapping positions along the observation area were defined and image acquisition was performed every 10 min for 24 h. Overlapping positions were afterwards stitched to one position using the IMAGEJ pairwise stitching plugin [57]. Sixty-seven single cells were tracked with the Manual tracking plugin in IMAGEJ. Chemotactic migration was confirmed by Rayleigh test. The chemotactic index, which represents the path towards the chemoattractant divided by the total path, was

17424658, 2023, 22, Downloaded from https://febs.onlinelibrary.wiley.com/doi/10.1111/febs.16912 by Universität Hohenheim, Wiley Online Library on [09/09/2026]. See the Terms and Conditions (https://onlinelibrary.wiley.com/terms-and-conditions) on Wiley Online Library for rules of use; OA articles are governed by the applicable Creative Commons License

calculated. Normal distribution of the data was verified, and groups were compared by one-sided *t*-test.

Co-immunoprecipitation

For co-IP, 1.14×10^6 HEK293T cells were seeded in 6-cm dishes and transfected the day after with 500 ng or, for the co-transfection, 1000 ng of the indicated plasmids. Twenty hours posttransfection, cells were harvested and lysed in 1 mL ice-cold lysis buffer (50 mM Tris/HCl pH 7.4, 150 mM NaCl, 1% NP40, 100 nM β-glycerophosphate, 100 nM sodium orthovanadate, 1 mM NaF and cOmplete Mini Protease inhibitor Cocktail (Roche, Mannheim, Germany) and incubated on ice for 10 min. Next, the lysate was centrifuged at 14 000 ***g*** for 20 min at 4 °C. Forty microlitres of the supernatant was saved as input sample for immunoblot before 10 µL of a 50% anti-flag M2 affinity gel slurry (Sigma-Aldrich) in PBS was added and gently mixed for 4 h at 4 °C. Afterwards, the beads were washed five times with ice-cold lysis buffer, before 20 µL of a two-fold Laemmli buffer was added. The input samples were lysed with 10 µL of a 5× Laemmli buffer, all samples were boiled at 95 °C for 10 min and analysed by SDS/PAGE and immunoblot.

Mass spectrometry

Mass spectrometry (MS) was performed as recently described [58]. Briefly, proteins were digested on beads using trypsin (Roche) in 6 M urea, 50 mM Tris–HCl pH 8.5. Cysteines were reduced using 1,4-dithiothreitol (DTT) and then alkylated by chloroacetamide. Samples were then diluted to a final concentration of 2 M urea. Seven hundred and fifty nanograms trypsin were added, and samples were digested overnight at 25 °C. The digests were stopped by adding trifluoroacetic acid (TFA). Next, peptide mixtures were concentrated and desalted on C18 stage tips and dried under vacuum. Samples were dissolved in 0.1% TFA and were subjected to nano LC–MS/MS analysis on an EASY-nLC 1000 system (Thermo Fisher Scientific) coupled to a Q-Exactive Plus mass spectrometer (Thermo Fisher Scientific) using an EASY-Spray nanoelectrospray ion source (Thermo Fisher Scientific). The was controlled by XCALIBUR 3.0.63 software (Thermo Fisher Scientific). Tryptic peptides were directly injected into a 25 cm × 75 µm EASY-Spray analytical column (2 µm, 100 Å, PepMap C18) operated at 35 °C. Peptides were separated at a flow rate of 250 $nL \cdot min^{-1}$ using a 120-min gradient with the following profile: 3–10% solvent B in 50 min, 10–22% solvent B in 40 min, 22–45% solvent B in 30 min, 45–90% solvent B in 10 min, 15-min isocratic at 90% solvent B, followed by 90–3% solvent B in 10 min and re-equilibration at 3% solvent B for 15 min [solvent A: 0.5% acetic acid; solvent B: acetonitrile/H_2O (80/20, v/v), 0.5% acetic acid].

MS spectra (m/z = 300–1600) were detected at a resolution of 70 000 (m/z = 200) using a maximum injection time (MIT) of 100 ms and an automatic gain control (AGC) value of 1×10^6. MS/MS spectra were generated for the 10 most abundant peptide precursors using high energy collision dissociation fragmentation at a resolution of 17 500, normalized collision energy of 27 and an intensity threshold of 1.3×10^5. Only ions with charge states from +2 to +5 were selected for fragmentation using an isolation width of 1.6 Da. For each MS/MS scan, the AGC was set at 5×10^5 and the MIT was 100 ms. MASCOT 2.6 (Matrix Science, London, UK) was used as search engine for protein identification. Spectra were searched against the human UniProt database (UniProt, 2021). SCAFFOLD 4.8.6. (Proteome Software, Portland, OR, USA) was used to evaluate peptide identifications. These were accepted with a peptide probability > 80% as specified by the PEPTIDE PROPHET algorithm [59]. Proteins had to be identified by at least one unique peptide and a protein probability of at least 99% to be accepted.

Cytokine quantification

IL-8 (CXCL8) release was measured in cell supernatants by ELISA (DY208; R&D System/Biotechne, Wiesbaden, Germany) according to the manufacturer's instructions.

Data presentation and analysis

Data were analysed and figures plotted with PYTHON 3 (Python Software Foundation, Wilmington, DE, USA). For statistical tests, the adequate function of the pingouin package was used as specified in the figure legends. Figures were assembled using INKSCAPE (BROOKLY, NY, USA).

Acknowledgements

We thank Yvonne Postma for technical assistance, Dr Timo Voß for critical reading of the manuscript and all members of the Kufer and Venturelli labs for helpful discussions. We thank Andrew Clark (University of Stuttgart) for advice on image analysis. AP was supported by a grant from Dr. Hans Fritz Stiftung. Open Access funding enabled and organized by Projekt DEAL.

Conflict of interest

The authors declare no conflict of interest.

Author contributions

LH, SB and KE planned, performed the experiments and analysed the data. FB wrote the scripts and analysed the data. SV and AP provided essential input on

17424658, 2023, 22, Downloaded from https://febs.onlinelibrary.wiley.com/doi/10.1111/febs.16912 by Universität Hohenheim, Wiley Online Library on [09/09/2026]. See the Terms and Conditions (https://onlinelibrary.wiley.com/terms-and-conditions) on Wiley Online Library for rules of use; OA articles are governed by the applicable Creative Commons License

the study and access to the xCELLigence RTCA device, TAK conceived and supervised the study, LH and TAK wrote the first draft of the manuscript. All authors edited the final version of the manuscript and agreed on submission.

Data availability statement

The data that supports the findings of this study are available in the figures and the Supporting Information of this article. The Script and Macro used for the analysis of the data are openly available on GitHub (https://github.com/KuferLabHohenheim/Woundhealing-Tool.git).

References

1 Janeway CA Jr & Medzhitov R (2002) Innate immune recognition. *Annu Rev Immunol* **20**, 197–216.
2 Chamaillard M, Hashimoto M, Horie Y, Masumoto J, Qiu S, Saab L, Ogura Y, Kawasaki A, Fukase K, Kusumoto S *et al.* (2003) An essential role for NOD1 in host recognition of bacterial peptidoglycan containing diaminopimelic acid. *Nat Immunol* **4**, 702–707.
3 Girardin SE, Travassos LH, Hervé M, Blanot D, Boneca IG, Philpott DJ, Sansonetti PJ & Mengin-Lecreulx D (2003) Peptidoglycan molecular requirements allowing detection by Nod1 and Nod2. *J Biol Chem* **278**, 41702–41708.
4 Inohara N, Koseki T, Del Peso L, Hu Y, Yee C, Chen S, Carrio R, Merino J, Liu D, Ni J *et al.* (1999) Nod1, an Apaf-1-like activator of caspase-9 and nuclear factor-kappaB. *J Biol Chem* **274**, 14560–14567.
5 Allison CC, Kufer TA, Kremmer E, Kaparakis M & Ferrero RL (2009) Helicobacter pylori induces MAPK phosphorylation and AP-1 activation via a NOD1-dependent mechanism. *J Immunol* **183**, 8099–8109.
6 Correia JDS, Miranda Y, Austin-Brown N, Hsu J, Mathison J, Xiang R, Zhou H, Li Q, Han J & Ulevitch RJ (2006) Nod1-dependent control of tumor growth. *Proc Natl Acad Sci USA* **103**, 1840–1845.
7 Wang X, Jiang W-H, Duan N, Qian Y-J, Zhou Q, Ye P, Jiang H, Bai Y, Zhang W & Wang W (2014) NOD1, RIP2 and Caspase12 are potentially novel biomarkers for oral squamous cell carcinoma development and progression. *Int J Clin Exp Pathol* **7**, 1677–1686.
8 Chen GY, Shaw MH, Redondo G & Nunez G (2008) Innate immune receptor nod1 protects the intestine from inflammation-induced tumorigenesis. *Cancer Res* **68**, 10060–10067.
9 Liu X, Ma H, Fei L, Jiang M, Xia M, Bai L, Pi X, Chen S & Yu L (2020) HPV-mediated down-regulation of NOD1 inhibits apoptosis in cervical cancer. *Infect Agent Cancer* **15**, 6.
10 Zhang Y, Li N, Yuan G, Yao H, Zhang D, Li N, Zhang G, Sun Y, Wang W, Zeng J *et al.* (2022) Upregulation of NOD1 and NOD2 contribute to cancer progression through the positive regulation of tumorigenicity and metastasis in human squamous cervical cancer. *BMC Med* **20**, 55.
11 Zhang WJ & Wang YY (2021) Activation of RIPK2-mediated NOD1 signaling promotes proliferation and invasion of ovarian cancer cells via NF-κB pathway. *Histochem Cell Biol* **157**, 173–182.
12 Liu R, Truax AD, Chen L, Hu P-Z, Li Z-S, Chen J, Song C-J, Chen L & Ting JP-Y (2015) Expression profile of innate immune receptors, NLRs and AIM2, in human colorectal cancer: correlation with cancer stages and inflammasome components. *Oncotarget* **6**, 33456–33469.
13 Jiang HY, Najmeh S, Martel G, MacFadden-Murphy E, Farias R, Savage P, Leone A, Roussel L, Cools-Lartigue J, Gowing S *et al.* (2020) Activation of the pattern recognition receptor NOD1 augments colon cancer metastasis. *Protein Cell* **11**, 187–201.
14 Maisonneuve C, Tsang DKL, Foerster EG, Robert LM, Mukherjee T, Prescott D, Tattoli I, Lemire P, Winer DA, Winer S *et al.* (2021) Nod1 promotes colorectal carcinogenesis by regulating the immunosuppressive functions of tumor-infiltrating myeloid cells. *Cell Rep* **34**, 108677.
15 Klein C, Grudzien M, Appaswamy G, Germeshausen M, Sandrock I, Schaffer AA, Rathinam C, Boztug K, Schwinzer B, Rezaei N *et al.* (2007) HAX1 deficiency causes autosomal recessive severe congenital neutropenia (Kostmann disease). *Nat Genet* **39**, 86–92.
16 Vafiadaki E, Arvanitis DA, Pagakis SN, Papalouka V, Sanoudou D, Kontrogianni-Konstantopoulos A & Kranias EG (2009) The anti-apoptotic protein HAX-1 interacts with SERCA2 and regulates its protein levels to promote cell survival. *Mol Biol Cell* **20**, 306–318.
17 Radhika V, Onesime D, Ji HH & Dhanasekaran N (2004) Gα13 stimulates cell migration through cortactin-interacting protein Hax-1. *J Biol Chem* **279**, 49406–49413.
18 Chao J-R, Parganas E, Boyd K, Hong CY, Opferman JT & Ihle JN (2008) Hax1-mediated processing of HtrA2 by Parl allows survival of lymphocytes and neurons. *Nature* **452**, 98–102.
19 Klein C (2017) Kostmann's disease and HCLS1-associated protein X-1 (HAX1). *J Clin Immunol* **37**, 117–122.
20 Wei X-J, Li S-Y, Yu B, Chen G, Du J-F & Cai H-Y (2014) Expression of HAX-1 in human colorectal cancer and its clinical significance. *Tumour Biol* **35**, 1411–1415.
21 Li F, Shang Y, Shi F, Zhang L, Yan J, Sun Q & She J (2020) Expression of integrin β6 and Hax-1 correlates with aggressive features and poor prognosis in

17424658, 2023, 22, Downloaded from https://febs.onlinelibrary.wiley.com/doi/10.1111/febs.16912 by Universität Hohenheim, Wiley Online Library on [09/09/2026]. See the Terms and Conditions (https://onlinelibrary.wiley.com/terms-and-conditions) on Wiley Online Library for rules of use; OA articles are governed by the applicable Creative Commons License

esophageal squamous cell carcinoma. *Cancer Manag Res* **12**, 9599–9608.
22 Li M, Tang Y, Zang W, Xuan X, Wang N, Ma Y, Wang Y, Dong Z & Zhao G (2013) Analysis of HAX-1 gene expression in esophageal squamous cell carcinoma. *Diagn Pathol* **8**, 47.
23 Trebinska A, Rembiszewska A, Ciosek K, Ptaszynski K, Rowinski S, Kupryjanczyk J, Siedlecki JA & Grzybowska EA (2010) HAX-1 overexpression, splicing and cellular localization in tumors. *BMC Cancer* **10**, 76.
24 Hu Y-L, Feng Y, Ma P, Wang F, Huang H, Guo Y-B, Li P, Mao Q-S & Xue W-J (2019) HAX-1 promotes the migration and invasion of hepatocellular carcinoma cells through the induction of epithelial–mesenchymal transition via the NF-κB pathway. *Exp Cell Res* **381**, 66–76.
25 Wu Z, Ai X, Hu H, Wang S, Wang Y, Kang F, Ouyang C & Zhu J (2019) Hematopoietic-substrate-1 associated protein X-1 (HAX-1) regulates liver cancer cells growth, metastasis, and angiogenesis through Akt. *Cancer Biol Ther* **20**, 1223–1233.
26 Gomathinayagam R, Jayaraman M, Ha JH, Varadarajalu L & Dhanasekaran DN (2014) Hax-1 is required for rac1-cortactin interaction and ovarian carcinoma cell migration. *Genes Cancer* **5**, 84–99.
27 Lin J, Wang Y & Lin Z (2021) HAX1 maintains the glioma progression in hypoxia through promoting mitochondrial fission. *J Cell Mol Med* **25**, 11170–11184.
28 Balcerak A, Trebinska-Stryjewska A, Wakula M, Chmielarczyk M, Smietanka U, Rubel T, Konopinski R, Macech-Klicka E, Zub R & Grzybowska EA (2019) HAX1 impact on collective cell migration, cell adhesion, and cell shape is linked to the regulation of actomyosin contractility. *Mol Biol Cell* **30**, 3024–3036.
29 Grada A, Otero-Vinas M, Prieto-Castrillo F, Obagi Z & Falanga V (2017) Research techniques made simple: analysis of collective cell migration using the wound healing assay. *J Invest Dermatol* **137**, e11–e16.
30 Friedl P & Wolf K (2003) Tumour-cell invasion and migration: diversity and escape mechanisms. *Nat Rev Cancer* **3**, 362–374.
31 Qin L, Yang D, Yi W, Cao H & Xiao G (2021) Roles of leader and follower cells in collective cell migration. *Mol Biol Cell* **32**, 1267–1272.
32 Olayioye MA, Barisic S & Hausser A (2013) Multi-level control of actin dynamics by protein kinase D. *Cell Signal* **25**, 1739–1747.
33 Bielig H, Lautz K, Braun PR, Menning M, Machuy N, Brügmann C, Barisic S, Eisler SA, Andree M, Zurek B *et al.* (2014) The cofilin phosphatase slingshot homolog 1 (SSH1) links NOD1 signaling to actin remodeling. *PLoS Pathog* **10**, e1004351.
34 Keestra AM, Winter MG, Auburger JJ, Fräßle SP, Xavier MN, Winter SE, Kim A, Poon V, Ravesloot MM, Waldenmaier JFT *et al.* (2013) Manipulation of small Rho GTPases is a pathogen-induced process detected by NOD1. *Nature* **496**, 233–237.
35 Zhang Y, Zhang X-F, Fleming MR, Amiri A, El-Hassar L, Surguchev AA, Hyland C, Jenkins DP, Desai R, Brown MR *et al.* (2016) Kv3.3 channels bind Hax-1 and Arp2/3 to assemble a stable local actin network that regulates channel gating. *Cell* **165**, 434–448.
36 Cavnar PJ, Berthier E, Beebe DJ & Huttenlocher A (2011) Hax1 regulates neutrophil adhesion and motility through RhoA. *J Cell Biol* **193**, 465–473.
37 Alekhina O & Marchese A (2016) β-Arrestin1 and signal-transducing adaptor molecule 1 (STAM1) cooperate to promote focal adhesion kinase autophosphorylation and chemotaxis via the chemokine receptor CXCR4. *J Biol Chem* **291**, 26083–26097.
38 Guo F, Wang Y, Liu J, Mok SC, Xue F & Zhang W (2016) CXCL12/CXCR4: a symbiotic bridge linking cancer cells and their stromal neighbors in oncogenic communication networks. *Oncogene* **35**, 816–826.
39 D'Agostino G, Artinger M, Locati M, Perez L, Legler DF, Bianchi ME, Rüegg C, Thelen M, Marchese A, Rocchi MBL *et al.* (2020) β-Arrestin1 and β-arrestin2 are required to support the activity of the CXCL12/HMGB1 heterocomplex on CXCR4. *Front Immunol* **11**, 2297.
40 Kufer TA, Kremmer E, Adam AC, Philpott DJ & Sansonetti PJ (2008) The pattern-recognition molecule Nod1 is localized at the plasma membrane at sites of bacterial interaction. *Cell Microbiol* **10**, 477–486.
41 Girardin SE, Tournebize R, Mavris M, Page AL, Li X, Stark GR, Bertin J, DiStefano PS, Yaniv M, Sansonetti PJ *et al.* (2001) CARD4/Nod1 mediates NF-kappaB and JNK activation by invasive *Shigella flexneri*. *EMBO Rep* **2**, 736–742.
42 Pei G, Zyla J, He L, Moura-Alves P, Steinle H, Saikali P, Lozza L, Nieuwenhuizen N, Weiner J, Mollenkopf H-J *et al.* (2021) Cellular stress promotes NOD1/2-dependent inflammation via the endogenous metabolite sphingosine-1-phosphate. *EMBO J* **40**, e106272.
43 Irving AT, Mimuro H, Kufer TA, Lo C, Wheeler R, Turner LJ, Thomas BJ, Malosse C, Gantier MP, Casillas LN *et al.* (2014) The immune receptor NOD1 and kinase RIP2 interact with bacterial peptidoglycan on early endosomes to promote autophagy and inflammatory signaling. *Cell Host Microbe* **15**, 623–635.
44 Travassos LH, Carneiro LA, Ramjeet M, Hussey S, Kim YG, Magalhaes JG, Yuan L, Soares F, Chea E, Le Bourhis L *et al.* (2010) Nod1 and Nod2 direct autophagy by recruiting ATG16L1 to the plasma membrane at the site of bacterial entry. *Nat Immunol* **11**, 55–62.
45 Zhang L, Huang Q-W, Pu Y-F, Xiao X-Q, Song B-J, Zhang X-P, Yang Y-S, Zhang Y-S & Gong F-H (2022) RIP2 knockdown attenuates vascular smooth muscle

17424658, 2023, 22, Downloaded from https://febs.onlinelibrary.wiley.com/doi/10.1111/febs.16912 by Universität Hohenheim, Wiley Online Library on [09/09/2026]. See the Terms and Conditions (https://onlinelibrary.wiley.com/terms-and-conditions) on Wiley Online Library for rules of use; OA articles are governed by the applicable Creative Commons License

cells activation via negative regulating myocardin expression. *Am J Hypertens* **35**, 454–461.
46 Girardin SE, Boneca IG, Viala J, Chamaillard M, Labigne A, Thomas G, Philpott DJ & Sansonetti PJ (2003) Nod2 is a general sensor of peptidoglycan through muramyl dipeptide (MDP) detection. *J Biol Chem* **278**, 8869–8872.
47 Philpott DJ, Sorbara MT, Robertson SJ, Croitoru K & Girardin SE (2014) NOD proteins: regulators of inflammation in health and disease. *Nat Rev Immunol* **14**, 9–23.
48 Gurses SA, Banskar S, Stewart C, Trimoski B, Dziarski R & Gupta D (2020) Nod2 protects mice from inflammation and obesity-dependent liver cancer. *Sci Rep* **10**, 20519.
49 Kwon MY, Liu X, Lee SJ, Kang YH, Choi AM, Lee KU, Perrella MA & Chung SW (2011) Nucleotide-binding oligomerization domain protein 2 deficiency enhances neointimal formation in response to vascular injury. *Arterioscler Thromb Vasc Biol* **31**, 2441–2447.
50 Fernández-García V, González-Ramos S, Avendaño-Ortiz J, Martín-Sanz P, Gómez-Coronado D, Delgado C, Castrillo A & Boscá L (2022) High-fat diet activates splenic NOD1 and enhances neutrophil recruitment and neutrophil extracellular traps release in the spleen of ApoE-deficient mice. *Cell Mol Life Sci* **79**, 396.
51 Kasimsetty SG, Hawkes A, Barekatain K, Soo E, Welch AK & McKay DB (2020) TLR2 and NODs1 and 2 cooperate in inflammatory responses associated with renal ischemia reperfusion injury. *Transpl Immunol* **58**, 101260.
52 Chan KL, Tam TH, Boroumand P, Prescott D, Costford SR, Escalante NK, Fine N, Tu Y, Robertson SJ, Prabaharan D *et al*. (2017) Circulating NOD1 activators and hematopoietic NOD1 contribute to metabolic inflammation and insulin resistance. *Cell Rep* **18**, 2415–2426.
53 Ellwanger K, Briese S, Arnold C, Kienes I, Heim V, Nachbur U & Kufer TA (2019) XIAP controls RIPK2 signaling by preventing its deposition in speck-like structures. *Life Sci Alliance* **2**, e201900346.
54 Vafiadaki E, Sanoudou D, Arvanitis DA, Catino DH, Kranias EG & Kontrogianni-Konstantopoulos A (2007) Phospholamban interacts with HAX-1, a mitochondrial protein with anti-apoptotic function. *J Mol Biol* **367**, 65–79.
55 Bäcker V (2012) ImageJ macro tool sets for biological image analysis. In Proceedings of the ImageJ User and Developer Conference, Luxembourg (Vol. **24**, p. 26).
56 Gebäck T, Schulz MMP, Koumoutsakos P & Detmar M (2009) TScratch: a novel and simple software tool for automated analysis of monolayer wound healing assays. *Biotechniques* **46**, 265–274.
57 Preibisch S, Saalfeld S & Tomancak P (2009) Globally optimal stitching of tiled 3D microscopic image acquisitions. *Bioinformatics* **25**, 1463–1465.
58 Kienes I, Bauer S, Gottschild C, Mirza N, Pfannstiel J, Schroder M & Kufer TA (2021) DDX3X links NLRP11 to the regulation of type I interferon responses and NLRP3 inflammasome activation. *Front Immunol* **12**, 653883.
59 Keller A, Nesvizhskii AI, Kolker E & Aebersold R (2002) Empirical statistical model to estimate the accuracy of peptide identifications made by MS/MS and database search. *Anal Chem* **74**, 5383–5392.

Supporting information

Additional supporting information may be found online in the Supporting Information section at the end of the article.

Movie S1. Representative movie of a wound healing assay showing the automated analysis with our macro.

17424658, 2023, 22, Downloaded from https://febs.onlinelibrary.wiley.com/doi/10.1111/febs.16912 by Universität Hohenheim, Wiley Online Library on [09/09/2026]. See the Terms and Conditions (https://onlinelibrary.wiley.com/terms-and-conditions) on Wiley Online Library for rules of use; OA articles are governed by the applicable Creative Commons License